

# Investigation of hardness in transition metal hexa-nitrides in cubic structure: A first-principles study

S.R. Kandel<sup>a</sup>, B.B. Dumre<sup>a</sup>, D. Gall<sup>b</sup>, S.V. Khare<sup>a,\*</sup>

<sup>a</sup> Department of Physics and Astronomy, University of Toledo, Toledo, OH, 43606, USA

<sup>b</sup> Department of Materials Science and Engineering, Rensselaer Polytechnic Institute, Troy, NY, 12180, USA

## ARTICLE INFO

### Keywords:

Transition metal nitrides  
Density functional theory  
Vickers hardness  
Electronic properties  
Vibrational properties

## ABSTRACT

We have studied all 29 transition metal nitrides (TMNs) of stoichiometric ratio 1:6 (M:N) in cubic structure (space group:  $Im\bar{3}m$ ) using density functional theory-based calculations. Our calculations include computations of structural, mechanical, vibrational, magnetic, energetic, thermal, and electronic properties. Our calculations indicate that only 5  $MN_6$  compounds are both vibrationally and mechanically stable. Out of them, the hardest compound  $CrN_6$  has Vickers hardness of 16 GPa. Higher hardness is directly proportional to higher mass density of the  $MN_6$ , whereas inversely proportional to M-M and M – N bond lengths. The band structure analysis shows that all the mechanically stable compounds except  $HgN_6$  are metallic in nature. The study of magnetic properties reveals that only 8 of  $MN_6$  have magnetic moment.

## 1. Introduction

Transition metal nitrides (TMNs) are being studied extensively for their outstanding mechanical properties, high hardness, chemical inertness, high melting point, high thermal conductivity, and varying electrical conductivity [1–10]. The measured values of hardness of many experimentally synthesized TMNs have revealed their potential applications in hard coatings [11–13]. Thus, these properties have enabled TMNs to become a material of growing interest for hard coating as well as semiconductor industries [11,14,15]. Besides experimental methods, theoretical and computational methods, such as first principles calculations, are now being used by many research groups to investigate the material properties [16–18]. The results obtained from those calculations are found to be in good agreement with the experimental data. Thus, such calculations help researchers to predict the stability and other novel properties of TMNs.

Various stoichiometric ratios of metal (M) and N have been proposed and studied for predicting higher hardness in TMNs [19–24]. Recently, Xia et al. [25] have proposed a machine learning algorithm of crystal structure search utilizing the first principles-based calculations that has been used to search for stable super-hard (Vickers hardness, ( $H_V$ ) > 40 GPa [26]) TMN compounds. In their study, they have predicted a super-hard tungsten (W) nitride in the stoichiometric ratio of 1:6 ( $WN_6$ ) which falls in hexagonal crystal structure of space group  $R\bar{3}m$  with

hexagonal axes which has  $H_V$  around 57 GPa. Li et al. [27] also have found nearly identical properties (average  $H_V = 54$  GPa) for the same  $WN_6$  in hexagonal crystal structure using intelligence-based Crystal Structure Analysis by the Particle Swarm Optimization (CALYPSO) algorithm. Due to this motivation, besides hexagonal  $WN_6$ , we recently expanded the study in  $MN_6$  for all 29 TMNs in the same hexagonal structure [28]. Besides hexagonal structure, Li et al. [27] also discovered the cubic structure (space group:  $Im\bar{3}m$ ) of  $WN_6$  while utilizing CALYPSO algorithm; this cubic phase  $MN_6$  will be called  $MN_6$  hereafter. The hardness for such  $WN_6$  has been proposed to be either 42.9 GPa calculated from a semi-empirical model [24,27], or 10.1 GPa computed from a theoretical model related to elasticity [20,27]. Motivated by all these works, besides  $WN_6$ , a holistic study of hardness and the reasons behind causing such hardness for all 29 TMN of stoichiometric ratio 1:6 (M:N) in cubic structure is necessary.

In this work, we have predicted the structural, vibrational, energetic, mechanical, thermal, electronic, and magnetic properties for nitrogen rich cubic phase of 29 TMN compounds of stoichiometric ratio 1:6 (M:N) by utilizing density functional theory (DFT). We have used an improved methodology in the calculation of Vickers hardness given by Tian et al. [29] as compared to the two varying low level theories [20,24] used earlier by Li et al. [27]. Our study reveals that only 5  $MN_6$  compounds are both mechanically and vibrationally stable. Out of those compounds, the softest compound ( $HfN_6$ ) has Vickers Hardness ( $H_V$ ) of 6 GPa,

\* Corresponding author.

E-mail address: [sanjay.khare@utoledo.edu](mailto:sanjay.khare@utoledo.edu) (S.V. Khare).

<https://doi.org/10.1016/j.jpcs.2022.111022>

Received 30 June 2022; Received in revised form 1 September 2022; Accepted 23 September 2022

Available online 30 September 2022

0022-3697/© 2022 Elsevier Ltd. All rights reserved.

whereas the hardest compound (CrN<sub>6</sub>) has  $H_V$  of 16 GPa. In each row, the group 6 MN<sub>6</sub> compounds possess the highest hardness owing to the half-filled d-orbitals of transition metals. All the compounds which are mechanically stable except HgN<sub>6</sub> are metallic in nature. Out of the 8 compounds that show magnetic properties, only one of them (TcN<sub>6</sub>) is both vibrationally and mechanically stable with 0.726  $\mu_B$  magnetic moment in unit cell.

## 2. Computational methods

Vienna Ab initio Simulation Package (VASP) is utilized for all the Density Functional Theory based calculations [30–40]. The electron density is approximated by using the Perdew-Burke-Ernzerhof (PBE) functional within Generalized Gradient Approximation (GGA) where the Projector Augmented Wave (PAW) method is implemented [36–44]. VASP pseudopotentials with the inner core electrons for all 29-transition metals where available, and N for nitrogen are considered [8,45–48]. The plane wave of cut off energy of 600 eV and gamma centered k-points grid of density  $9 \times 9 \times 9$  are used for relaxation. Electronic and ionic convergence criteria are  $10^{-6}$  eV and 0.01 eV/Å respectively with Gaussian smearing of width 0.1 eV [41,45,48]. The initial structure of MN<sub>6</sub> is taken from the work of Li et al. [27].

Formation energy per formula unit of M<sub>x</sub>N<sub>y</sub>, where x and y are positive integers corresponding to relevant TMN, is calculated as:

$$E_f = E(M_xN_y) - xE(M) - yE(N_2) / 2 \quad (1)$$

where,  $E(M_xN_y)$ ,  $E(M)$ , and  $E(N_2)$  are the ground state energies of TMN, transition metal, and nitrogen dimer in vacuo [8]. All ground state energies were obtained from full relaxation of relevant unit cells of TMN (space group:  $Im\bar{3}m$ ), transition metals with lowest  $E_f$  as obtained from Materials Project [49], and a nitrogen dimer placed in a large cubic cell of length 10 Å. Further, study on the thermodynamic stability of our hardest compound CrN<sub>6</sub> was done by comparing the  $E_f$  of different nitride phases of chromium, such as CrN (space group:  $P\bar{6}m2$ ), Cr<sub>2</sub>N (space group:  $P\bar{3}1m$ ), and CrN<sub>2</sub> (space group:  $Pnm$ ).

To study the mechanical properties, we have calculated the Hessian matrix using finite differences. The limiting strain of 0.015 Å was utilized in the process of calculating the stress-strain relationship. Elastic moduli are calculated by using the following set of equations involving components of stiffness ( $C_{ij}$ ) and compliance ( $S_{ij}$ ) tensors as suggested by Voigt-Reuss-Hill approximations [50–52]. Subscripts V and R respectively denote Voigt and Reuss approximations for bulk modulus ( $B$ ) and shear modulus ( $G$ ).

$$B_V = [(C_{11} + C_{22} + C_{33}) + 2(C_{12} + C_{23} + C_{31})] / 9 \quad (2)$$

$$G_V = [(C_{11} + C_{22} + C_{33}) - (C_{12} + C_{23} + C_{31}) + 3(C_{44} + C_{55} + C_{66})] / 15 \quad (3)$$

$$B_R = [(S_{11} + S_{22} + S_{33}) + 2(S_{12} + S_{23} + S_{31})]^{-1} \quad (4)$$

$$G_R = 15[4(S_{11} + S_{22} + S_{33}) - 4(S_{12} + S_{23} + S_{31}) + 3(S_{44} + S_{55} + S_{66})]^{-1} \quad (5)$$

$$B = (B_V + B_R) / 2 \text{ and } G = (G_V + G_R) / 2 \quad (6)$$

Based on the values of  $B$ ,  $G$ , and Pugh's ratio ( $k = G/B$ ), the Vickers hardness is calculated using equation suggested by Tian et al. [36–38, 53–55] as:

$$H_V = 0.92k^{1.137}G^{0.708} \quad (7)$$

The values of  $B$  and  $G$  also enables to calculate Poisson's ratio,  $\nu = (3 - 2k)/(6 + 2k)$ , (8)

$$\text{and Young's modulus, } E = 9G \backslash / (3 + k) \quad (9)$$

According to Deus and Schneider, Debye temperature ( $\theta_D$ ) may be estimated as:

$$\theta_D = aH_V^{1/2}\rho^{-1/6}M^{-1/3} + b \quad (10)$$

where,  $a$  and  $b$  are linear fitting constants,  $M$  is molecular weight, and  $\rho$  is mass density of the material [45,56]. Debye temperature for material having  $n$  atoms in unit cell may be related to transverse ( $v_t = \sqrt{G/\rho}$ ) and longitudinal ( $v_l = \sqrt{(3B + 4G)/3\rho}$ ) component of speed of sound as [45,54,57]:

$$\theta_D = \frac{h}{k_B} \left[ \frac{3n}{4\pi} \left( \frac{\rho N_A}{M} \right) \right]^{1/3} \left[ \frac{1}{3} \left( \frac{2}{v_t^3} + \frac{1}{v_l^3} \right) \right]^{-1/3} \quad (11)$$

where,  $h$  is Plank's constant,  $k_B$  is Boltzmann's constant, and  $N_A$  is Avogadro's number.

Electronic properties are studied from electronic Local Density Of States (LDOS) and band structure [58]. Phonon Density Of States (DOS) are calculated to check the vibrational stability and Crystal Orbital Hamilton Population (COHP) for the bonding relationship between the atoms in the compound [23,36,59–63]. Bader charge analysis is employed for the calculation of charge transfer ( $Q_t$ ) from metal to nitrogen [64–67].

## 3. Result and discussion

### 3.1. Structural and vibrational properties

The crystal structure of MN<sub>6</sub> (space group  $Im\bar{3}m$ ) prepared with the help of Visualization for Electronic and Structural Analysis (VESTA) [68] is shown in Fig. 1. This structure has octahedral geometry with Wyckoff positions of M and N at  $2a$  (0.0, 0.0, 0.0) and  $12e$  (0.108, 0.500, 0.500) respectively. For all 29 TMNs, the calculated value of  $\rho$  of compounds varies from 2158 kg/m<sup>3</sup> to 6510 kg/m<sup>3</sup> shown in Table 1, and N–N bond length varies from 1.117 Å to 1.168 Å shown in Table 2. Also, from Tables 1 and 2, we can observe the higher hardness is attributed to higher densities for 3d, 4d and 5d compounds, however, it is unclear to see the relationship of hardness to the N–N bond length (Supplementary Fig. S1 (a)). Supplementary Fig. S1 (b) and S1 (c) show that for harder materials, M – N and M–M bond lengths are less than that for softer materials. Table 1 displays the calculated values of  $E_f$  for all 29 MN<sub>6</sub> where only 8 of them are negative, remaining all are positive indicating that most of the MN<sub>6</sub> materials can be prepared by endothermic

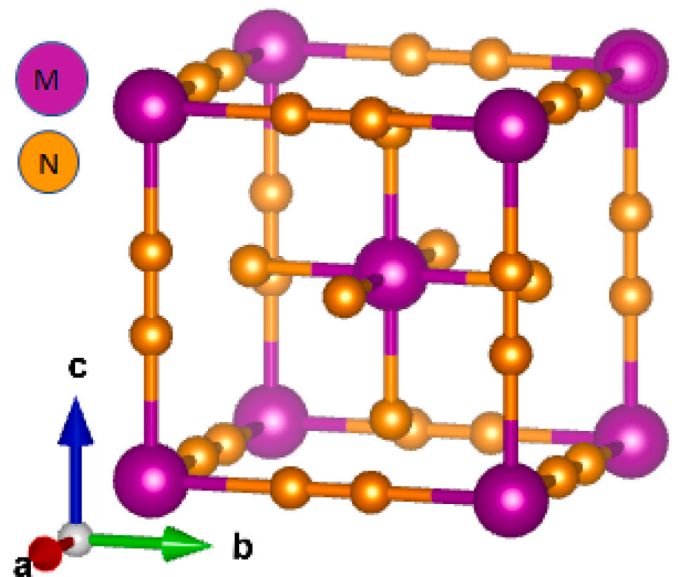


Fig. 1. Cubic MN<sub>6</sub> structure prepared by using VESTA [68]. Crystallographic directions are given by a, b, and c.

**Table 1**

Lattice constant ( $a$ ), elastic constants ( $C_{11}$ ,  $C_{12}$  and  $C_{44}$ ), charge transfer from metal to nitrogen ( $Q_t$ ) in units of elementary charge  $e$ , formation energy ( $E_f$ ) per atom, mass density ( $\rho$ ), mechanical stability, and total magnetic moment (Mag.), per transition metal atom, in Bohr magneton ( $\mu_B$ ) of all MN<sub>6</sub> compounds. “S” and “U” respectively denote the mechanically stable and unstable compounds.

Group No.	M	$a$ (Å)	$C_{11}$ (GPa)	$C_{12}$ (GPa)	$C_{44}$ (GPa)	$Q_t$ ( $e$ )	$E_f$ (eV)	$\rho$ kg/m <sup>3</sup>	Mechanical Stability	Mag. ( $\mu_B$ )
3	Sc	5.612	241	46	28	1.75	-0.10	2423	S	0
4	Ti	5.364	271	75	45	1.71	-0.06	2837	S	0
5	V	5.216	408	39	67	1.73	-0.01	3158	S	0
6	Cr	5.143	437	30	71	1.49	0.06	3320	S	0
7	Mn	5.200	256	68	60	1.35	0.16	3284	S	0
8	Fe	5.340	169	77	48	1.08	0.21	3050	S	0
9	Co	5.490	69	26	36	1.00	0.24	2868	S	-1.540
10	Ni	5.656	92	64	32	0.68	0.23	2619	S	0
11	Cu	5.724	94	50	24	0.94	0.25	2613	S	0.046
12	Zn	5.528	167	68	29	1.31	0.30	2936	S	0
3	Y	5.866	240	39	21	1.98	-0.11	2845	S	0
4	Zr	5.596	292	72	34	2.06	-0.10	3320	S	0
5	Nb	5.406	444	43	56	1.97	-0.05	3718	S	0
6	Mo	5.308	495	33	62	1.71	0.02	3996	S	0
7	Tc	5.239	505	36	53	1.61	0.15	4204	S	-0.051
8	Ru	5.509	57	91	38	1.11	0.30	3675	U	0
9	Rh	5.907	45	74	26	0.69	0.27	3011	U	0.989
10	Pd	5.459	195	116	16	0.67	0.57	3887	S	0
11	Ag	6.243	69	33	14	0.76	0.23	2618	S	0.027
12	Cd	6.711	86	0	4	0.15	0.30	2158	S	0
4	Hf	5.515	357	72	38	2.12	-0.08	5196	S	0
5	Ta	5.367	512	51	60	2.15	-0.03	5690	S	0
6	W	5.274 5.19 <sup>a</sup>	585 687 <sup>a</sup>	36 40 <sup>a</sup>	67 50 <sup>a</sup>	1.94	0.06	6062	S	0
7	Re	5.226	621	42	51	1.64	0.18	6288	S	-0.037
8	Os	5.191	573	36	50	1.66	0.36	6510	S	0
9	Ir	5.191	-33	113	26	0.82	0.43	4683	U	1.140
10	Pt	6.097	25	74	18	0.41	0.35	4089	U	0
11	Au	6.497	25	6	7	0.04	0.34	3402	S	0.455
12	Hg	7.029	75	11	8	0.06	0.15	2721	S	0

<sup>a</sup> Theoretical Ref. [27].

**Table 2**

Bulk modulus ( $B$ ), shear modulus ( $G$ ), Young's modulus ( $E$ ), Vickers hardness ( $H_V$ ), Pugh's ratio ( $k$ ), Poisson's ratio ( $\nu$ ), Debye temperature ( $\theta_D$ ), and N-N bond length for mechanically stable MN<sub>6</sub> compounds.

Group No.	M	$B$ (GPa)	$G$ (GPa)	$E$ (GPa)	$H_V$ (GPa)	$k$	$\nu$	$\theta_D$ (K)	N-N bond length (Å)
3	Sc	111	47	125	5	0.43	0.31	633	1.152
4	Ti	140	62	162	7	0.44	0.31	698	1.154
5	V	162	102	253	14	0.63	0.24	867	1.153
6	Cr	166	110	270	16	0.66	0.23	889	1.149
7	Mn	131	72	182	10	0.55	0.27	718	1.149
8	Fe	108	47	124	6	0.44	0.31	591	1.144
9	Co	40	29	71	7	0.73	0.21	461	1.138
10	Ni	73	23	62	2	0.31	0.36	423	1.132
11	Cu	65	23	62	3	0.36	0.34	419	1.137
12	Zn	101	36	96	4	0.36	0.34	510	1.152
3	Y	106	42	111	4	0.39	0.33	525	1.154
4	Zr	145	56	148	5	0.38	0.33	589	1.159
5	Nb	177	96	244	12	0.54	0.27	751	1.159
6	Mo	187	109	273	14	0.58	0.26	783	1.153
7	Tc	192	101	258	12	0.53	0.28	748	1.157
10	Pd	142	23	66	1	0.16	0.42	365	1.127
11	Ag	45	15	42	2	0.34	0.35	314	1.135
12	Cd	29	13	34	2	0.45	0.30	292	1.117
4	Hf	167	67	177	6	0.40	0.32	522	1.163
5	Ta	205	107	273	12	0.52	0.28	645	1.164
6	W	219 255.7 <sup>a</sup>	123 117.3 <sup>a</sup>	311 682.7 <sup>a</sup>	14 10.1 <sup>a</sup>	0.56	0.26	681	1.161
7	Re	235	111	288	11	0.47	0.30	645	1.162
8	Os	215	106	273	11	0.49	0.29	621	1.168
11	Au	12	8	20	2	0.64	0.24	187	1.120
12	Hg	32	15	38	2	0.45	0.30	263	1.148

<sup>a</sup> Theoretical Ref. [27].

chemical reaction. The  $E_f$  of the hardest material CrN<sub>6</sub> in our study is +0.07 eV/atom. We have tried to further understand its relative formability by calculating the  $E_f$  of different nitride phases of chromium such as CrN ( $E_f = -0.54$  eV/atom), Cr<sub>2</sub>N ( $E_f = -0.41$  eV/atom), and CrN<sub>2</sub> ( $E_f = -0.07$  eV/atom). Hence, we can observe that CrN is the most

thermodynamically stable among these four compounds. It can be concluded that during the synthesis of CrN<sub>6</sub>, CrN will form first followed by Cr<sub>2</sub>N and then CrN<sub>2</sub> leading to CrN<sub>6</sub>. The synthesis of such materials can be possible with high pressure and temperature environment as it can be seen in the synthesis of PtN by Gregoryanz et al. [69] and PtN<sub>2</sub> by Jonathan C. Crowhurst et al. [70] where the high pressure of 50 GPa and

temperature of 2000 K were used. The synthesized material was stable even at ambient conditions. We have studied the volume of each unit cell ( $V$ ) and their  $E_f$  with the group numbers as shown in Fig. 2(a) and (c).  $E_f$  starts from the negative value and increases with group number, attains the maximum, and then decreases (see Fig. 2(a)). However, the volume decreases with group number and reaches its minimum and then increases with group number (see Fig. 2(c)). This variation of volume with group numbers could be due to the size of transition metals decreases from initial to intermediate elements and starts increasing thereafter [71].

We have computed the vibrational properties of a crystal via phonon frequency calculations as it provides the basis for thermal stability of the crystal in conjunction with mechanical stability. The results for phonon frequency calculation are shown in Fig. 3 where we can observe only 5 compounds ( $\text{HfN}_6$ ,  $\text{TcN}_6$ ,  $\text{MoN}_6$ ,  $\text{WN}_6$ , and  $\text{CrN}_6$ ) do not have phonon DOS in the imaginary phonon frequency region indicating them as vibrationally stable materials. We also observe a gap of around 30–40 THz in frequency of these stable materials above around 20 THz. This gap can help these materials to be used also as sound filters and mirrors as any frequency within the gap will not traverse in the material and thus gets reflected from its surface [72]. The phonon frequency calculation for only mechanically stable and thermally unstable materials is shown in Supplementary Figs. S2–1 and that for both mechanically and vibrationally unstable materials are shown in Supplementary Figs. S2–2. These figures indicate all other materials as vibrationally unstable which is confirmed by the presence of phonon DOS in the imaginary frequency region. Besides this, we do not observe any special trend in the only mechanically stable materials as shown in Supplementary Figs. S2–1. However, some gap, similar to the vibrationally stable case in Fig. 3, is observed in the case of mechanically unstable materials as well, as shown in Supplementary Figs. S2–2.

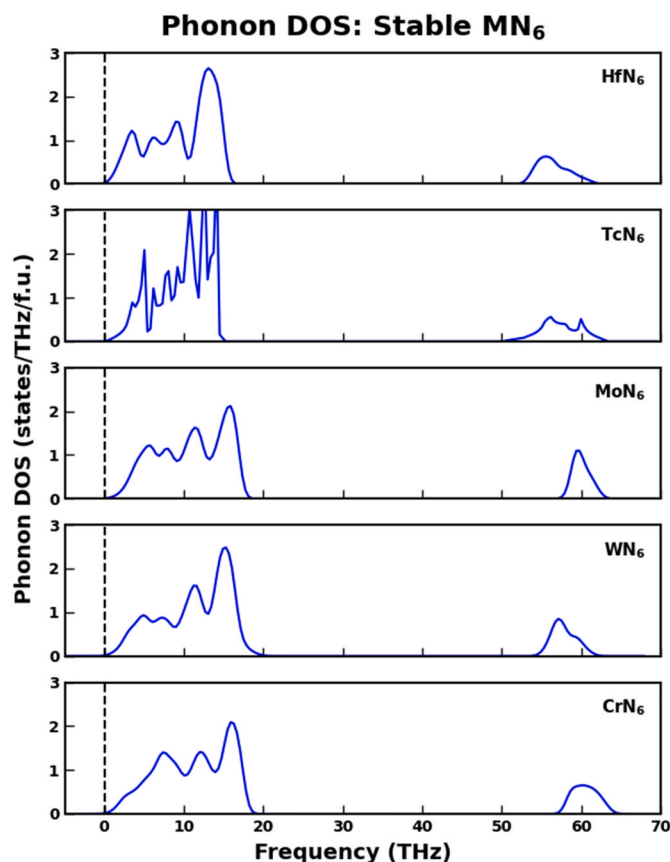


Fig. 3. Comparison of phonon DOS for both mechanically and vibrationally stable  $\text{MN}_6$  compounds in the order of increasing hardness from top to bottom.

### 3.2. Mechanical and magnetic properties

To predict the values of  $B$ ,  $G$ , and  $H_V$ , we used equations (2)–(7). Components of elastic compliance tensor ( $S_{ij}$ ) were obtained by taking the inverse matrix of elastic stiffness tensor ( $C_{ij}$ ) obtained from VASP calculation. Table (1) shows the calculated value of lattice constant ( $a$ ) and three independent elastic constants ( $C_{11}$ ,  $C_{12}$ , and  $C_{44}$ ) for all 29  $\text{MN}_6$  compounds. These calculated values of elastic constants were used to predict the mechanical stability of materials given by the following sets of equations as [73,74]:

$$C_{11} > C_{12}, C_{11} + 2C_{12} > 0, \text{ and } C_{44} > 0 \quad (12)$$

All the  $\text{MN}_6$  materials that satisfy the conditions described by equation (12) are mechanically stable. Our results of calculations of elastic moduli for such mechanically stable compounds are presented in Table (2). It shows the calculated hardness values first increases and attains the maximum value (16 GPa for 3d, 14 GPa for 4d, and 14 GPa for 5d compounds) and then decreases. The maximum  $H_V$  is observed at group 6 compounds for all materials, which could be due to the exact filling of half of the d-orbitals in these group 6 compounds. The earlier available theoretically calculated elastic properties and lattice constant by Li et al. [27], closely matched with our calculated values for cubic  $\text{WN}_6$  except for our predicted value of  $E$  (311 GPa) with the reported value of 682.7 GPa. To explain this difference, we used the reported values of  $C_{11}$ ,  $C_{12}$ , and  $C_{44}$  by Li et al. in equation (9) and re-calculated  $E$ . We found the newly calculated value of  $E$  is around 305.6 GPa and this is close to our result. We also studied the variation of  $G$ ,  $k$ ,  $H_V$ , and  $B$  with group number; the result is shown in Fig. 4. It shows  $G$ ,  $H_V$ , and  $B$  varies parabolically with group number whereas for  $k$ , the pattern is parabolic at first but after group 8, it is zig-zag in nature for all mechanically stable  $\text{MN}_6$  compounds. It is also observed that all vibrationally stable

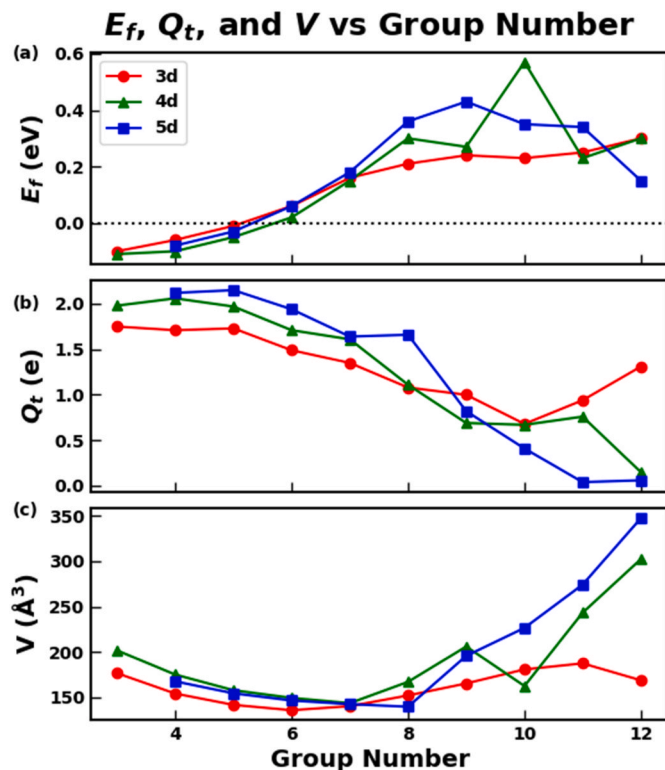


Fig. 2. The variation of  $E_f$ ,  $Q_t$ , and  $V$  with group number for all  $\text{MN}_6$  compounds.

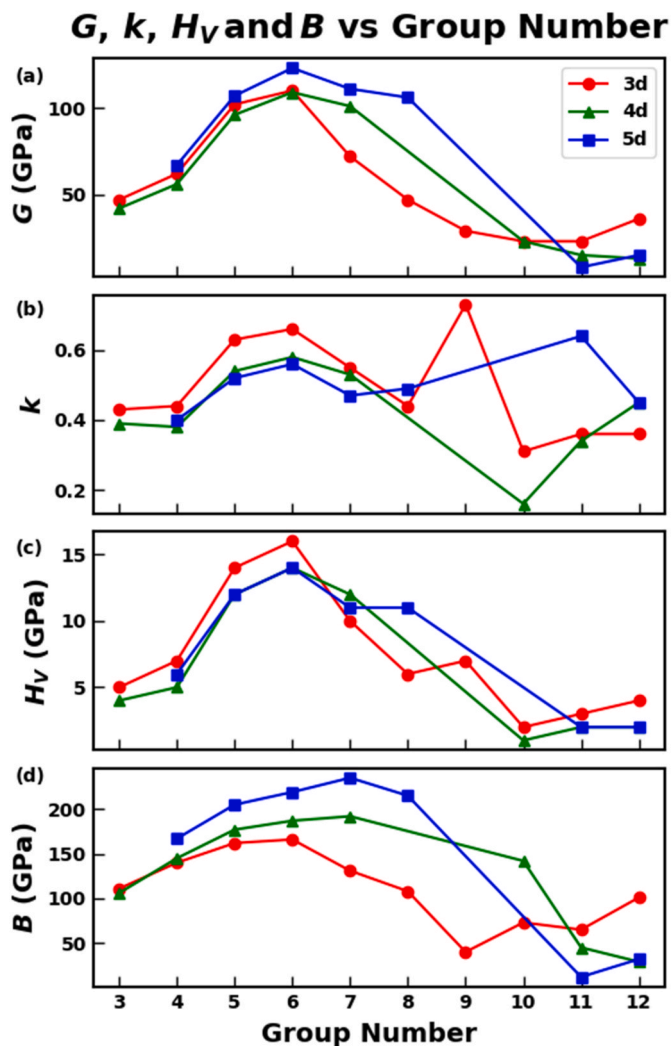


Fig. 4. The variation of  $G$ ,  $k$ ,  $H_V$ , and  $B$  with group number for mechanically stable MN<sub>6</sub> compounds.

compounds are mechanically stable as well indicating that only these materials are quenchable to ambient pressure. Since the elastic constant  $C_{44}$  and  $G$  may be related to the material's ability against shear deformations [34,35,75], we studied the variation of  $B$ ,  $G$ ,  $E$ , and  $H_V$  with  $C_{44}$  and the result is shown in Fig. 5 for all mechanically stable MN<sub>6</sub>. For 4d- and 5d-compounds, all elastic moduli are found to be increasing for increasing values of  $C_{44}$  while for 3d-compounds this is true only after  $C_{44} > 50$  GPa. However, among all mechanically stable MN<sub>6</sub>, the overall trend of  $H_V$  is increasing with increasing values of  $C_{44}$ . The calculated values of  $k$  determines whether the material is ductile ( $k \leq 0.57$ ) or brittle ( $k > 0.57$ ) [51,76–78]. Our study shows that most of the mechanically stable MN<sub>6</sub> materials are ductile in nature and is presented in Table 2.

Table 2 also presents the calculated values of  $\theta_D$  for all mechanically stable MN<sub>6</sub> compounds by using equation (11). Since equation (9) relies on  $v_t$  and  $v_l$  which are indeed calculated from  $B$  and  $G$ , the predicted values of  $\theta_D$  in this way purely depends on the mechanical properties only. We studied the relationship of predicted  $\theta_D$  and  $H_V$  by comparing the linear fit of equation (10) against calculated  $\theta_D$  as shown in Fig. 6. Fig. 6 shows that the materials with  $\theta_D$  less than 500 K are scattered more from the fitted line and most of these materials have hardness less than 10 GPa. In contrast, the materials with  $\theta_D$  higher than 500 K and higher hardness are less scattered. Thus, the material with higher  $\theta_D$  agrees with the estimate of Deus [56] and Miao et al. [79] where they

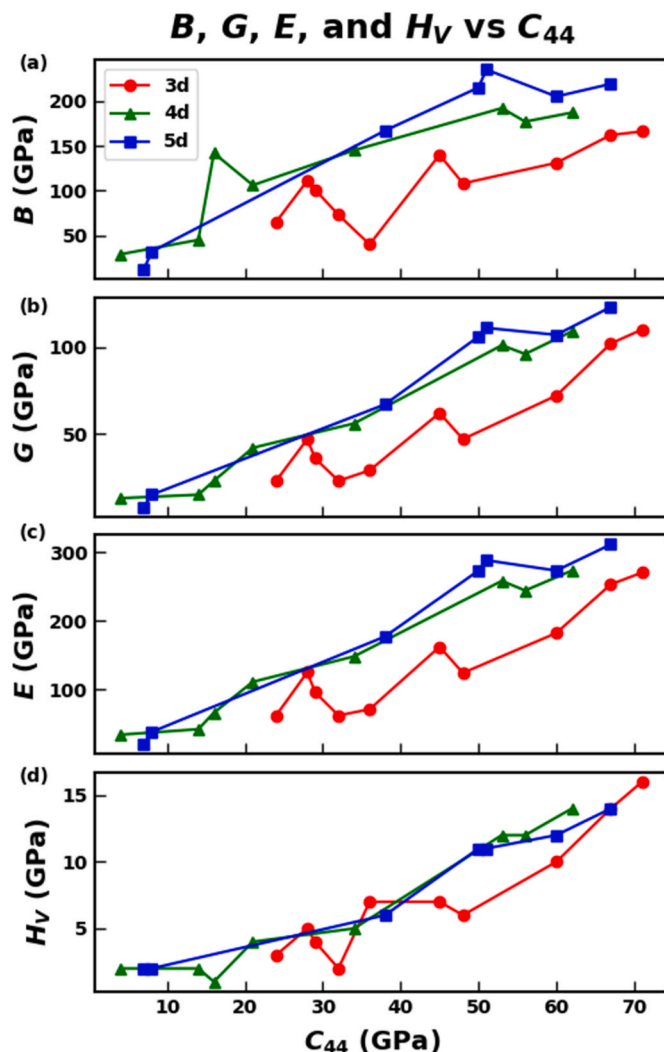


Fig. 5. Variation of  $B$ ,  $G$ ,  $E$ , and  $H_V$  with  $C_{44}$  for mechanically stable MN<sub>6</sub> compounds.

have predicted that  $\theta_D$  and  $H_V$  have linear relationship as described by equation (10). In our study the predicted values of fitting constants  $a$  and  $b$  are found to be  $5452.08 \text{ (GPa}^{-1/2}(\text{kg/m}^3)^{1/6}(\text{g/mol})^{1/3}\text{K)}$  and  $63.44 \text{ (K)}$  respectively.

Our calculations for magnetic moment of atomic orbitals are presented in Table S1. Out of all 29 TMNs, only 8 have shown the presence of magnetism and only one (TcN<sub>6</sub>) is both vibrationally and mechanically stable with magnetic moment  $0.726 \mu_B$  in unit cell. TcN<sub>6</sub>, CoN<sub>6</sub> and ReN<sub>6</sub>, are showing ferrimagnetic character. The remaining 5 MN<sub>6</sub> show ferromagnetic behavior. Out of the total contribution to the magnetic moment in all 8 MN<sub>6</sub>, the contribution in M atoms can be observed being dominated from d-orbital compared to s- and p-orbitals except in AuN<sub>6</sub> where s-orbital is dominant compared to p- and d-orbitals. Similarly, the magnetic moment in N atoms is contributed mainly from p-orbital compared to s-orbital.

### 3.3. Electronic properties

The study of charge transfer enables us to know the nature of bonding which may be related to the mechanical properties [80]. For all 29 MN<sub>6</sub>, we performed the Bader charge analysis and the result of charge transfer ( $Q_t$ ) from M to N is presented in Table 1. The study of  $Q_t$  with group number as presented in Fig. 2b shows a decrement in charge transfer for higher group numbers for all 3d, 4d, and 5d row elements

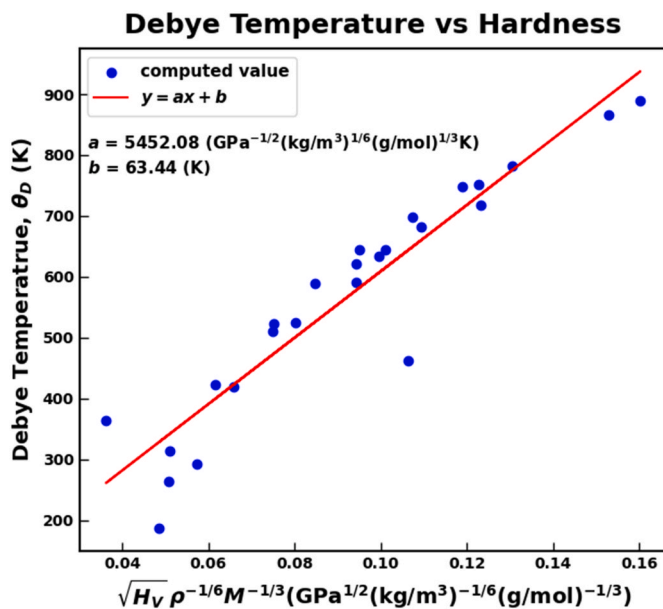


Fig. 6. Relation between  $\theta_D$  and a hardness parameter for mechanically stable  $MN_6$  compounds.

except for 3d elements there is little rise in  $Q_t$  after group 11. This decrement could be due to the filling of d-orbital as we move right in the period. Whenever d-count is more, M atoms may have less opportunity to provide electrons to N atoms than in M atoms with lower d-count because lower d-count M atoms are not able to fill their d-states completely in turn lending electrons to N atoms in  $MN_6$ . Also, for  $MN_6$  up to group 8 of all blocks, the charge transfer value is more than 1 e that confirms the electrovalent nature of the bonds in them, whereas for  $MN_6$  above group 8 has charge transfer value less than 1 e determining the electrovalent nature of bonds, except for the last member of 3-d block ( $ZnN_6$ ). Table S2 presents the values of electronegativity ( $\chi$ ) of transition metals taken from Ref. [81]. The values of charge transfer (see Table 1) are found to be anti-correlated with electronegativity as expected. Finally, we did not see any direct relationship between  $\chi$  or  $Q_t$  with  $H_V$ .

Fig. 7 shows the result for LDOS calculations for both mechanically and dynamically stable compounds in increasing order of hardness from top to bottom. It can be seen when observing from softest compound  $HfN_6$  ( $H_V = 6$  GPa) to hardest compound  $CrN_6$  ( $H_V = 16$  GPa), LDOS above Fermi level shift towards left and is continuous through the Fermi level showing its metallic character. For mechanically and vibrationally stable compounds at Fermi level, population of nitrogen LDOS is higher than the population of metallic LDOS, except in the softest compound  $HfN_6$ . Higher nitrogen LDOS possibly indicates the higher number of covalent repulsions between N–N atoms at Fermi level increases the overall hardness. This trend of having higher nitrogen LDOS at Fermi level is also true for harder compounds which are only mechanically stable (Supplementary Figs. S3–1). This higher nitrogen LDOS population at the Fermi level creates anti-bonding states causing harder compounds as will be discussed in detail in the following paragraph. However, for both vibrationally and mechanically unstable compounds, the metallic LDOS is higher around Fermi level (Supplementary Figs. S3–2).

The analysis of bonding and anti-bonding states of M and N atoms were done with the calculation of -pCOHP for all 29  $MN_6$  structures. The result of our calculations for both mechanically and vibrationally stable compounds in the order of increasing hardness is presented in Fig. 8. Here, anti-bonding is represented by -pCOHP population and bonding is represented by positive -pCOHP population below Fermi energy. It is evident from Fig. 8, S4-1 and S4-2 that for harder materials, all N–N (red line), M – N (blue line), and total (purple line) interactions are

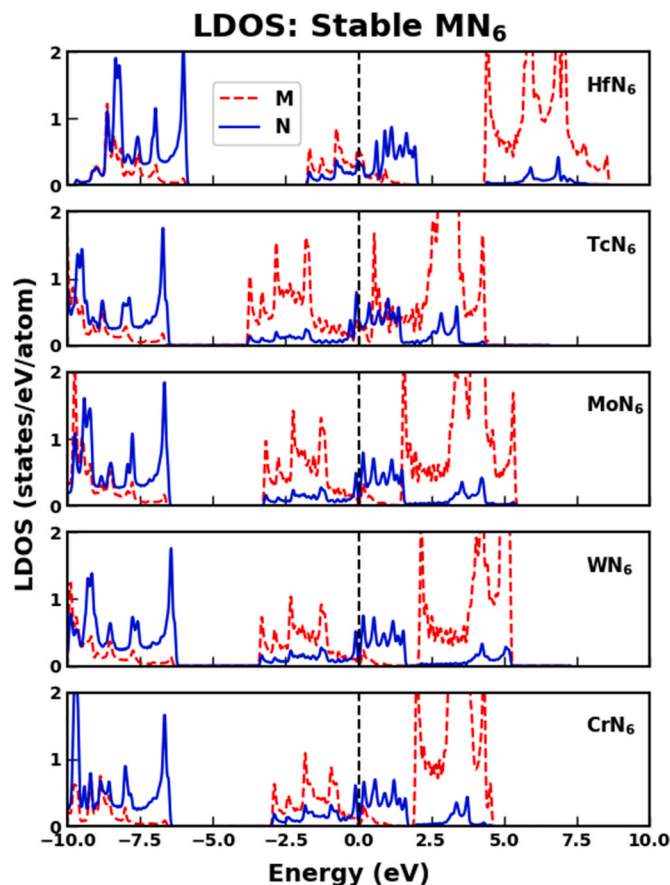


Fig. 7. Comparison of LDOS for both mechanically and vibrationally stable  $MN_6$  compounds in the order of increasing hardness from top to bottom. The Fermi level is set at 0 eV.

consistently similar in bonding and anti-bonding states at and deep below the Fermi level. For example, the M – N interaction has some bonding states right at the Fermi level, whereas the N–N interaction has some anti-bonding states near the Fermi level and a large bonding area deep below the Fermi level. However, this is not true for softer materials where such trend is not observed as shown in Figs. S4–1.

The calculation of electronic band structure using GGA functional for both vibrationally and mechanically stable  $MN_6$  compounds is presented in Fig. 9. Supplementary Figs. S5–1 (a), S5-1 (b), and S5-2 respectively represent the calculated band structure for only mechanically stable and both mechanically and vibrationally unstable  $MN_6$  compounds. It is evident from the calculations that for mechanically stable compounds, 24 cubic  $MN_6$  materials have zero band gap energy and possess metallic character except  $HgN_6$  has band gap of 1.754 eV. This can be verified from the LDOS calculations showing population of metallic LDOS at Fermi level. The highest hardness observed in  $MN_6$  is only 16 GPa ( $CrN_6$ ), which is considered low compared to others used in hard-coatings industry such as TiN (25 GPa), ZrC (27 GPa), HfN (20 GPa), TaC (26 GPa), etc. [5,41,82–84]. The metallic character could be the reason for low hardness observed because studies have shown that the increase in metallicity would decrease the material's hardness [24,85].

#### 4. Conclusion

In conclusion, all 29 cubic  $MN_6$  materials were studied using DFT based first principles calculations. Only 5 of these ( $HfN_6$ ,  $TcN_6$ ,  $MoN_6$ ,  $WN_6$ , and  $CrN_6$ ) are both mechanically and vibrationally stable and all others are dynamically unstable where some of them are both vibrationally and mechanically unstable. For those which are vibrationally

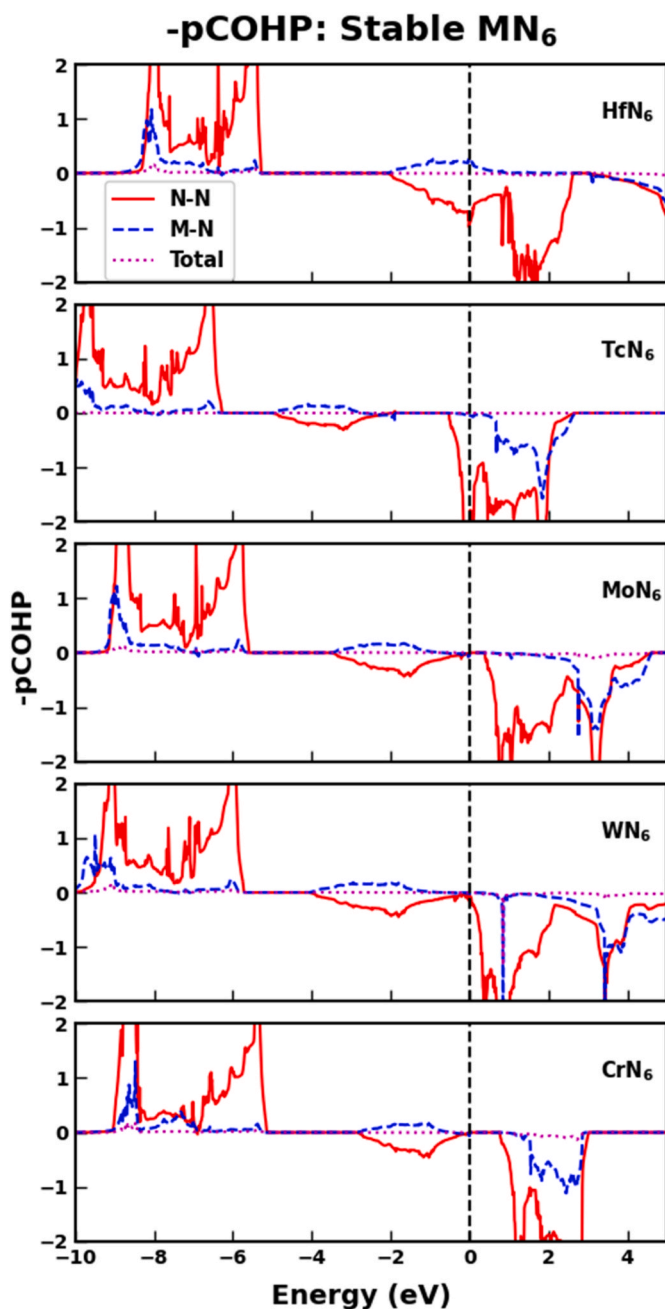


Fig. 8. Comparison of -pCOHP for both mechanically and vibrationally stable  $MN_6$  compounds in the order of increasing hardness from top to bottom. The Fermi level is set at 0 eV.

and mechanically stable, the softest compound ( $HfN_6$ ) has  $B = 167$  GPa,  $G = 67$  GPa, and  $H_V = 6$  GPa, and the hardest compound ( $CrN_6$ ) has  $B = 166$  GPa,  $G = 110$  GPa, and  $H_V = 16$  GPa. It has been observed that a higher hardness is directly proportional to higher mass density of the  $MN_6$ , whereas inversely proportional to M-M and M – N bond lengths. Calculation of LDOS and band structure analysis shows that all the materials which are mechanically stable possess metallic character having zero band gap energy except  $HgN_6$  which has a band gap of 1.754 eV. The nature of charge transfer from metal to nitrogen decreases with increasing group number. Our study also concludes that the compounds from group 6 elements are the hardest ones due to the filling of half d-orbitals. We observed magnetism in 8 compounds with only one of them ( $TcN_6$ ) being both vibrationally and mechanically stable indicating the hardest materials are non-magnetic.

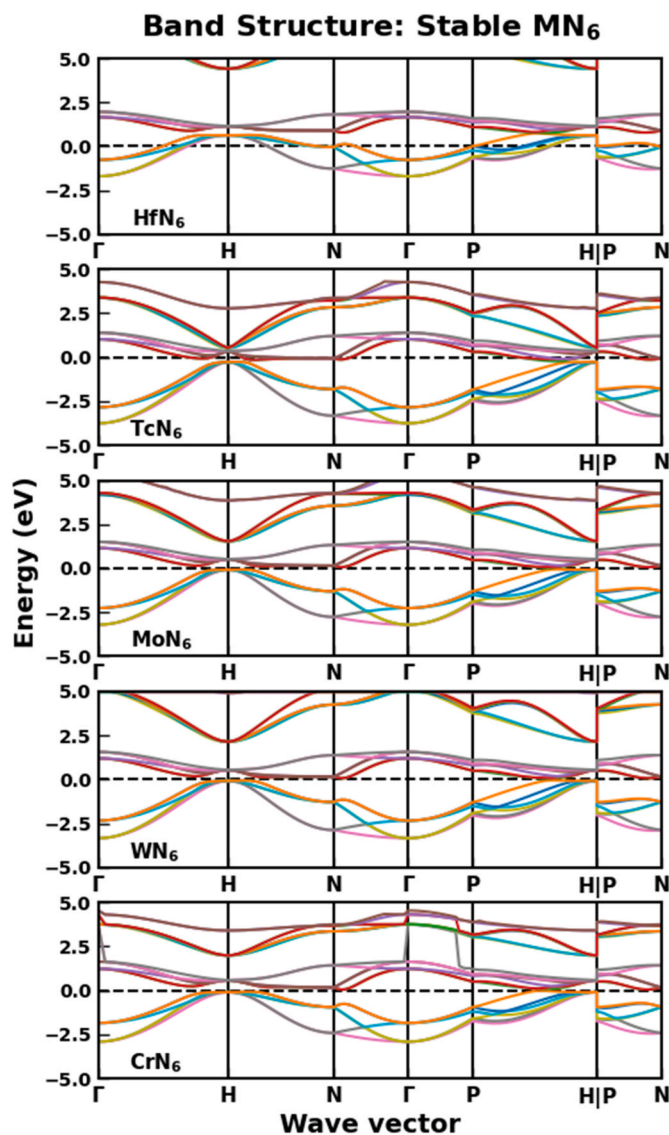


Fig. 9. Electronic band structure curves for both mechanically and vibrationally stable  $MN_6$  compounds in the order of increasing hardness from top to bottom. The Fermi level is set at 0 eV.

#### Author statement

**S. R. Kandel:** Investigation, Software, Writing-Original Draft. **B. B. Dumre:** Software, Validation, Writing-Review and Editing. **D. Gall:** Writing-Review and Editing, Funding Acquisition. **S. V. Khare:** Supervision, Funding Acquisition.

#### Declaration of competing interest

The authors declare that they have no known competing financial interests or personal relationships that could have appeared to influence the work reported in this paper.

#### Data availability

No data was used for the research described in the article.

#### Acknowledgements

The computational work for this project was performed at Ohio

Supercomputer Center [86]. We also thank National Science Foundation Division of Civil, Mechanical, and Manufacturing Innovation through grants 1629239 and 1629230 to support this work.

## Appendix A. Supplementary data

Supplementary data to this article can be found online at <https://doi.org/10.1016/j.jpcs.2022.111022>.

## References

- J.G. Zhao, et al., *Structural phase transition of Cu<sub>3</sub>N under high pressure*, Solid State Commun. 150 (33–34) (2010) 1521–1524.
- S.H. Jhi, et al., *Electronic mechanism of hardness enhancement in transition-metal carbonitrides*, Nature 399 (1999) 132–134.
- S.H. Jhi, et al., *Vacancy hardening and softening in transition metal carbides and nitrides*, Phys. Rev. Lett. 86 (15) (2001) 3348–3351.
- X.J. Chen, et al., *Hard superconducting nitrides*, Proc. Natl. Acad. Sci. U.S.A. 102 (2005) 3198–3201.
- S. Kodambaka, et al., *Absolute orientation-dependent anisotropic TiN(111) island step energies and stiffnesses from shape fluctuation analyses*, Phys. Rev. B 67 (3) (2003), 035409.
- A.M.Y.Y. Liu, Marvin L. Cohen, *Prediction of new low compressibility solids*, Science 245 (4920) (1989), 841–8420.
- Z.T.Y. Liu, et al., *First-principles investigation of the structural, mechanical and electronic properties of the NbO-structured 3d, 4d and 5d transition metal nitrides*, Comput. Mater. Sci. 84 (2014) 365–373.
- V. Adhikari, et al., *First-principles study of mechanical and magnetic properties of transition metal (M) nitrides in the cubic M<sub>4</sub>N structure*, J. Phys. Chem. Solid. 120 (2018) 197–206.
- H. Holleck, *Material selection for hard coatings*, J. Vac. Sci. Technol. 4 (1986) 2661.
- D. Gall, et al., *Growth of poly- and single-crystal ScN on MgO (001): role of low-energy N<sub>2</sub><sup>+</sup> irradiation in determining texture, microstructure evolution, and mechanical properties*, J. Appl. Phys. 84 (1998) 6034–6041.
- Haihua Chen, et al., *Strength and elastic moduli of TiN from radial x-ray diffraction under nonhydrostatic compression up to 45 GPa*, J. Appl. Phys. 107 (11) (2010), 113503.
- C.S. Shin, et al., *Vacancy hardening in single-crystal TiN<sub>x</sub>(001) layers*, J. Appl. Phys. 93 (10) (2003) 6025–6028.
- S. Kodambaka, et al., *Size-dependent detachment-limited decay kinetics of two-dimensional TiN islands on TiN(111)*, Phys. Rev. Lett. 89 (17) (2002), 176102.
- Akira Kobayashi, *Formation of TiN coatings by gas tunnel type plasma reactive spraying*, Surf. Coating. Technol. 132 (2000) 152–157.
- J. Baroño, et al., *TiN Surface Dynamics Role of Surface and Bulk Mass Transport Processes*, vol. 885, American Institute of Physics, 2007, pp. 205–224.
- S.V. Khare, T.L. Einstein, *Energetics of steps and kinks on Ag and Pt using equivalent crystal theory (ECT)*, Surf. Sci. 314 (1994) L857–L865.
- N.J. Szymanski, et al., *Electronic and optical properties of vanadium oxides from first principles*, Comput. Mater. Sci. 146 (2018) 310–318.
- I. Efthimiopoulos, et al., *Pressure-induced transition in the multiferroic CoCr<sub>2</sub>O<sub>4</sub> spinel*, Phys. Rev. B 92 (6) (2015), 064108.
- Z. Zhao, et al., *Nitrogen concentration driving the hardness of rhenium nitrides*, Sci. Rep. 4 (2014) 4797.
- Chen Xing-Qiu, et al., *Modeling hardness of polycrystalline materials and bulk metallic glasses*, Intermetallics 19 (9) (2011) 1275–1281.
- Zhonglong Zhao, et al., *Potentially superhard hcp CrN<sub>2</sub> compound studied at high pressure*, Phys. Rev. B 93 (21) (2016), 214104.
- K. Li, et al., *Electronegativity identification of novel superhard materials*, Phys. Rev. Lett. 100 (23) (2008), 235504.
- Z.T.Y. Liu, D. Gall, S.V. Khare, *Electronic and bonding analysis of hardness in pyrite-type transition-metal pernitrides*, Phys. Rev. B 90 (13) (2014), 134102.
- Xiaoju Guo, et al., *Hardness of covalent compounds: roles of metallic component and d valence electrons*, J. Appl. Phys. 104 (2) (2008), 023503.
- Xia Kang, et al., *A novel superhard tungsten nitride predicted by machine-learning accelerated crystal structure search*, Sci. Bull. 63 (13) (2018) 817–824.
- H.J. McSkimin, W.L. Bond, *Elastic moduli of diamond*, Phys. Rev. 105 (1) (1957) 116–121.
- Li Qian, et al., *New multifunctional tungsten nitride with energetic N<sub>6</sub> and extreme hardness predicted from first principles*, EPL 118 (4) (2017), 46001p1-p.5.
- S.R. Kandel, et al., *Prediction of super hardness in transition metal hexa-nitrides from density functional theory computations*, Materialia 25 (2022), 101550.
- Y. Tian, B. Xu, Z. Zhao, *Microscopic theory of hardness and design of novel superhard crystals*, Int. J. Refract. Metals Hard Mater. 33 (2012) 93–106.
- S.K.R. Patil, et al., *Mechanical stability of possible structures of PtN investigated using first-principles calculations*, Phys. Rev. B 73 (10) (2006), 104118.
- Yuejian Wang, et al., *Thermal equation of state of silicon carbide*, Appl. Phys. Lett. 108 (6) (2016), 061906.
- P.P. Gunaicha, et al., *Structural, energetic and elastic properties of Cu<sub>2</sub>ZnSn(S<sub>x</sub>Se<sub>1-x</sub>)<sub>4</sub> (x=1, 0.75, 0.5, 0.25, 0) alloys from first-principles computations*, Sol. Energy 102 (2014) 276–281.
- G. Kresse, J. Hafner, *Ab initio molecular dynamics for liquid metals*, Phys. Rev. B Condens. Matter 47 (1) (1993) 558–561.
- G. Kresse, J. Furthmuller, *Efficient iterative schemes for ab initio total-energy calculations using a plane-wave basis set*, Phys. Rev. B 54 (1996), 11169.
- G. Kresse, J. Furthmuller, *Efficiency of ab-initio total energy calculations for metals and semiconductors using a plane-wave basis set*, Comput. Mater. Sci. 6 (1996) 15–50.
- B.B. Dumre, D. Gall, S.V. Khare, *Stability, and electronic and optical properties of ternary nitride phases of MgSnN<sub>2</sub>: a first-principles study*, J. Phys. Chem. Solid. 153 (2021), 110011.
- B.B. Dumre, et al., *Improved optoelectronic properties in CdSe<sub>x</sub>Te<sub>1-x</sub> through controlled composition and short-range order*, Sol. Energy 194 (2019) 742–750.
- V. Adhikari, et al., *First principles investigation into the phase stability and enhanced hardness of TiN-ScN and TiN-YN alloys*, Thin Solid Films 688 (2019), 137284.
- N.J. Szymanski, et al., *Unconventional superconductivity in 3d rocksalt transition metal carbides*, J. Mater. Chem. C 7 (40) (2019) 12619–12632.
- G. Kresse, J. Hafner, *Ab initio molecular-dynamics simulation of the liquid-metal-amorphous-semiconductor transition in germanium*, Phys. Rev. B Condens. Matter 49 (20) (1994) 14251–14269.
- B.B. Dumre, S.V. Khare, *Interrelationship of bonding strength with structural stability of ternary oxide phases of MgSnO<sub>3</sub>: a first-principles study*, Phys. B Condens. Matter 637 (2022), 413896.
- John P. Perdew, Kieron Burke, M. Ernzerhof, *Generalized gradient approximation made simple*, Phys. Rev. Lett. 77 (1996) 3865–3868.
- P.E. Blochl, *Projector augmented-wave method*, Phys. Rev. B Condens. Matter 50 (24) (1994) 17953–17979.
- G. Kresse, D. Joubert, *From ultrasoft pseudopotentials to the projector augmented-wave method*, Phys. Rev. B 59 (1999) 1758–1775.
- Xiquan Zhou, Gall Daniel, V. Khare Sanjay, *Mechanical properties and electronic structure of anti-ReO<sub>3</sub> structured cubic nitrides, M<sub>3</sub>N, of d block transition metals M: An ab initio study*, J. Alloys Compd. 595 (2014) 80–86.
- J.L. Roehl, et al., *Binding sites and diffusion barriers of a Ga adatom on the GaAs (001)-c(4×4) surface from first-principles computations*, Phys. Rev. B 82 (16) (2010), 165335.
- J.A. Warner, et al., *Ab initio calculations for properties of MAX phases Ti<sub>2</sub>TiC, Zr<sub>2</sub>TiC, and Hf<sub>2</sub>TiC*, Appl. Phys. Lett. 88 (10) (2006), 101911.
- Nanke Jiang, et al., *An ab initio computational study of pure Zn<sub>3</sub>N<sub>2</sub> and its native point defects and dopants Cu, Ag and Au*, Thin Solid Films 564 (2014) 331–338.
- Anubhav Jain, et al., *Commentary: the Materials Project: a materials genome approach to accelerating materials innovation*, Apl. Mater. 1 (1) (2013), 011002.
- R. Hill, *The elastic behaviour of a crystalline aggregate*, Proc. Phys. Soc. 65 (1952) 349–354.
- Wei Qun, et al., *High-pressure phases and pressure-induced phase transition of MoN<sub>6</sub> and ReN<sub>6</sub>*, Phys. Lett. 383 (20) (2019) 2429–2435.
- Zhi-jian Wu, et al., *Crystal structures and elastic properties of superhard IrN<sub>2</sub> and IrN<sub>3</sub> from first principles*, Phys. Rev. B 76 (5) (2007), 054115.
- Yongjun Tian, Bo Xu, Zhisheng Zhao, *Microscopic theory of hardness and design of novel superhard crystals*, Int. J. Refract. Metals Hard Mater. 33 (2012) 93–106.
- Z.T. Liu, et al., *Structural, mechanical and electronic properties of 3d transition metal nitrides in cubic zincblende, rocksalt and cesium chloride structures: a first-principles investigation*, J. Phys. Condens. Matter 26 (2) (2014), 025404.
- V.T. Barone, et al., *Optoelectronic and mechanical properties of the orthorhombic and tetragonal Cu<sub>2</sub>CdGe(S<sub>x</sub>Se<sub>1-x</sub>)<sub>4</sub> semiconducting system via first principles methods*, J. Appl. Phys. 131 (20) (2022), 205701.
- P. Deus, H.A. Schneider, *Estimation of the debye temperature of diamond-like semiconducting compounds from bulk modul and microhardness*, Cryst. Res. Technol. 18 (1983) 491–500.
- W. Bao, D. Liu, Y. Duan, *A first-principles prediction of anisotropic elasticity and thermal properties of potential superhard WB<sub>3</sub>*, Ceram. Int. 44 (12) (2018) 14053–14062.
- Ruopeng Deng, et al., *Optical and transport measurement and first-principles determination of the ScN band gap*, Phys. Rev. B 91 (4) (2015), 045104.
- Atsushi Togo, Isao Tanaka, *First principles phonon calculations in materials science*, Scripta Mater. 108 (2015) 1–5.
- N.J. Szymanski, et al., *Prediction of improved magnetization and stability in Fe<sub>16</sub>N<sub>2</sub> through alloying*, J. Appl. Phys. 126 (9) (2019), 093903.
- R. Dronskowski, P.E. Bloch, *Crystal orbital Hamilton populations (COHP). Energy-resolved visualization of chemical bonding in solids based on density-functional calculations*, J. Phys. Chem. 97 (33) (1993) 8617–8624.
- S. Maintz, et al., *LOBSTER: a tool to extract chemical bonding from plane-wave based DFT*, J. Comput. Chem. 37 (11) (2016) 1030–1035.
- S. Maintz, M. Esser, R. Dronskowski, *Efficient rotation of local basis functions using real spherical harmonics*, Acta Phys. Pol. B 47 (4) (2016) 1165–1175.
- Henkelman Graeme, Arnaldsson Andri, Jónsson Hannes, *A fast and robust algorithm for Bader decomposition of charge density*, Comput. Mater. Sci. 36 (3) (2006) 354–360.
- M. Yu, D.R. Trinkle, *Accurate and efficient algorithm for Bader charge integration*, J. Chem. Phys. 134 (6) (2011), 064111.
- E. Sanville, et al., *Improved grid-based algorithm for Bader charge allocation*, J. Comput. Chem. 28 (5) (2007) 899–908.
- W. Tang, E. Sanville, G. Henkelman, *A grid-based Bader analysis algorithm without lattice bias*, J. Phys. Condens. Matter 21 (8) (2009), 084204.
- Momma Koichi, Izumi Fujio, *VESTA 3 for three-dimensional visualization of crystal, volumetric and morphology data*, J. Appl. Crystallogr. 44 (6) (2011) 1272–1276.
- Eugene Gregoryanz, et al., *Synthesis and characterization of a binary noble metal nitride*, Natural Materials 3 (2004) 294–297.

- [70] Jonathan C. Crowhurst, et al., Synthesis and characterization of the nitrides of platinum and iridium, *Science* 311 (5765) (2006) 1275–1278.
- [71] I. Khatri, et al., Correlating structure and orbital occupation with the stability and mechanical properties of 3d transition metal carbides, *J. Alloys Compd.* 891 (2022), 161866.
- [72] R.M. Hornreich, et al., Phonon band gaps, *J. Phys.* 7 (3) (1997) 509–519.
- [73] J.F. Nye, *Physical Properties of Crystals: Their Representation by Tensors and Matrices*, Oxford Science Publications, 1985.
- [74] Félix Mouhat, François-Xavier Coudert, Necessary and sufficient elastic stability conditions in various crystal systems, *Phys. Rev. B* 90 (22) (2014), 224104.
- [75] S.K.R. Patil, et al., Super hard cubic phases of period VI transition metal nitrides: first principles investigation, *Thin Solid Films* 517 (2) (2008) 824–827.
- [76] X. Jiang, J. Zhao, X. Jiang, Correlation between hardness and elastic moduli of the covalent crystals, *Comput. Mater. Sci.* 50 (7) (2011) 2287–2290.
- [77] S.F. Pugh, Relations between the elastic moduli and the plastic properties of polycrystalline pure metals, *Philos. Mag. J. Sci.* 45 (1954) 823–843.
- [78] A. Mansouri Tehrani, et al., Machine learning directed search for ultraincompressible, superhard materials, *J. Am. Chem. Soc.* 140 (31) (2018) 9844–9853.
- [79] N.H. Miao, et al., *Theoretical investigation on the transition metal borides with Ta<sub>3</sub>B<sub>4</sub>-type structure a class of hard and refractory material*, *Comput. Mater. Sci.* 50 (2011) 1559–1566.
- [80] F. Gao, et al., Hardness of covalent crystals, *Phys. Rev. Lett.* 91 (1) (2003), 015502.
- [81] A.L. Allred, E.G. Rochow, A scale of electronegativity based on electrostatic force, *J. Inorg. Nucl. Chem.* 5 (1958) 264–268.
- [82] K. Balasubramanian, S.V. Khare, D. Gall, Valence electron concentration as an indicator for mechanical properties in rocksalt structure nitrides, carbides and carbonitrides, *Acta Mater.* 152 (2018) 175–185.
- [83] B.D. Ozsdolay, et al., Cubic  $\beta$ -WN layers: growth and properties vs N-to-W ratio, *Surf. Coating. Technol.* 304 (2016) 98–107.
- [84] J. Baréno, et al., Orientation-dependent mobilities from analyses of two-dimensional TiN(111) island decay kinetics, *Thin Solid Films* 510 (1–2) (2006) 339–345.
- [85] Qianqian Wang, et al., Is orthorhombic iron tetraboride superhard? *J. Materiom.* 1 (1) (2015) 45–51.
- [86] Ohio Supercomputer Center. 1987.